Locating fixed points in the phase plane

Yanhua Zhang,[1] Yeyin Zhao,[1] Lizhu Chen,[2] Xue Pan,[3] Mingmei Xu,[1] Zhiming Li,[1] Yu Zhou,[4] and Yuanfang Wu[1,*]

[1]*Key Laboratory of Quark and Lepton Physics (MOE) and Institute of Particle Physics, Central China Normal University, Wuhan 430079, China*

[2]*School of Physics and Optoelectronic Engineering, Nanjing University of Information Science and Technology, Nanjing 210044, China*

[3]*School of Electronic Engineering, Chengdu Technological University, Chengdu 611730, China*

[4]*No.1 Middle School Affiliated to Central China Normal University, Wuhan 430223, China*

(Received 30 May 2019; published 27 November 2019)

The critical point is a fixed point in finite-size scaling. To quantify the behavior of such a fixed point, we define, at a given temperature and scaling exponent ratio, the width of scaled observables for different sizes. The minimum of the width reveals the position of the fixed point, its corresponding phase transition temperature, and scaling exponent ratio. The value of this ratio tells the nature of the fixed point, which can be a critical point, a point of the first-order phase transition line, or a point of the crossover region. To demonstrate the effectiveness of this method, we apply it to three typical samples produced by the three-dimensional three-state Potts model. Results show the method to be more precise and effective than conventional methods. Finally, we discuss a possible application at the Beam Energy Scan program of the Relativistic Heavy Ion Collider.

DOI: 10.1103/PhysRevE.100.052146

I. INTRODUCTION

The phase diagram in statistical physics labels the boundary where a phase transition (PT) happens. In order to draw this boundary with precision, some key points of the boundary line should be located first. The critical point (CP) of the second-order PT is one of these points. Its temperature, the so-called critical temperature (T_C), is one of the most interesting parameters [1–8].

As we know, if the volume of the system is large enough, T_C can be approximately determined by the peak position of the distribution of susceptibility [9–11], whereas for the system with finite volume, T_C has to be determined by the finite-size scaling (FSS) [1,2,12–15].

The FSS of observable $Q(T, L)$ has usually the form [12,13]

$$Q(T, L) = L^{-\lambda/\nu} f_Q(tL^{1/\nu}), \tag{1}$$

where $t = (T - T_C)/T_C$ is the reduced temperature, f_Q is a scaling function, $tL^{1/\nu}$ is a scaled variable, and λ and ν are respectively the scaling exponents of the observable and the correlation length $\xi \propto |\tau|^{-\nu}$. These exponents characterize the universal class of PTs. Here the scaling exponent ratio (SER) $a = \lambda/\nu$ is *a fraction* between the spatial dimension d and zero.

The FSS means that the observables for different system sizes and temperatures can be scaled to a universal scaling function, as shown in Fig. 1(a). There are three parameters, T_C, ν, and λ (or a), in this scaling function. To determine T_C and scaling exponents, it is usually assumed that the observables fall in a certain universal class. T_C is obtained by the Binder cumulant ratio, and scaling exponents are obtained by the best scaling plot of the observables of different sizes [16–18]. Selection of the best scaling is done through visual observation. The method, therefore, often lacks precision [19].

On the other hand, the FSS also implies a *fixed point* (FP). If we plot the scaled observable versus T, instead of the scaled variable $tL^{1/\nu}$, the curves of different sizes will intersect at the FP, where $T = T_C$ and the scaling function $f_Q(0)$ is independent of system size [i.e., Fig. 1(b)]. The parameter ν is therefore omitted in this plot.

The FP is obtained from the scale transformation of the renormalization group [13,20,21]. In a phase diagram, not only is the CP a FP, but also the point of the first-order PT line [13,22–24] [cf. Figs. 1(c) and 1(d)]. The SER a of the first-order PT line is an *integer*, in contrast to that of the second-order PT, where a is a fraction.

It is clear that the scaling holds in a limited range of system size or temperature, as shown in Figs. 1(a) and 1(c). The valid range of size or temperature varies with the system studied, its spatial dimension, and the order of PT. For a relatively small size or a substantial deviation from the critical temperature, the scaling is violated. So with the change of size or temperature, there should be a correction for the scaling. However, as the scaled variable is the product of reduced temperature and size, the temperature and size are tied together in the scaling plot. The influence of size or temperature is therefore difficult to quantify.

In contrast to the scaling plots in Figs. 1(a) and 1(c), the plots of FP in Fig. 1(b) and 1(d) show clearly how scaled observables for different sizes vary with temperature. Any deviation from the critical (or transitional) temperature, and the curves for different sizes are separate from each other. They converge, or intersect only at the critical (or transitional) temperature. This feature allows us to quantify the deviation for different sizes at a given temperature, and to accurately locate the critical temperature.

*wuyf@mail.ccnu.edu.cn

 ©2019 American Physical Society

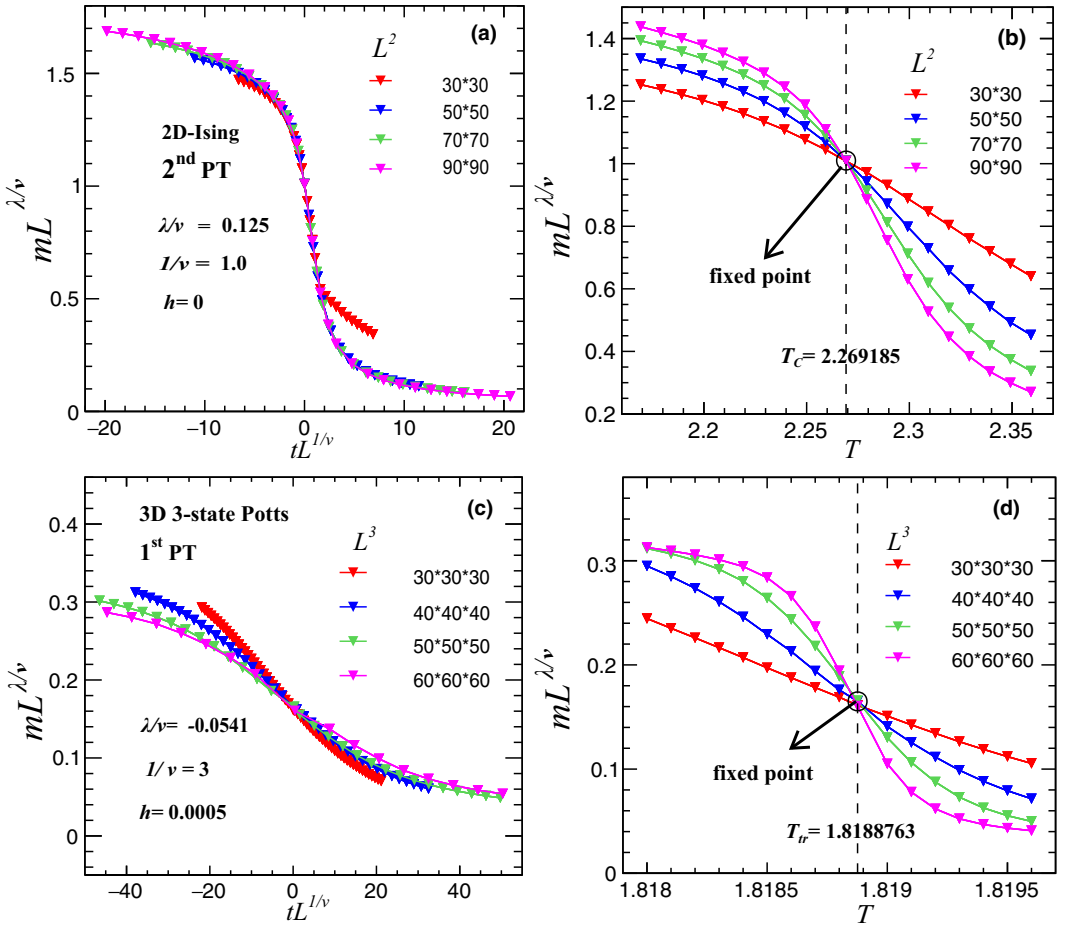

FIG. 1. The scaled order parameter ($mL^{\lambda/\nu}$) versus (a, c) the scaled variable ($tL^{1/\nu}$) and (b, d) T for the (a, b) second-order (2D Ising model with external field $h = 0$) and (c, d) first-order PTs (3D three-state Potts model with $h = 0.0005$), respectively.

At a given T and a, all points of curves for different sizes can be regarded as a set. The width of the set can be defined as the square root of the variance of scaled observables. Usually, the defined width depends on T and a. When T and a both approach transition values, all points in the set overlap within error, i.e., the FP, and the defined width reaches its minimum. So defined width well quantifies the behavior of the FP. $T_{\rm FP}$ and $a_{\rm FP}$ can be determined by the minimization of the width.

For the crossover region, the observable is independent of system size in the region of transition temperature [25]. This character can be generalized to SER $a = 0$ in scaling form Eq. (1). It implies that curves for different sizes, as those shown in Figs. 1(b) and 1(d), overlap within errors at the region of transition temperature. The defined width is therefore also minimized, the same as in the case of the FP.

Therefore, in general, the value of $a_{\rm FP}$ reveals the nature of the FP, which is either a CP, a point of the first-order PT line, or a point of the crossover region.

In this paper, we first quantify the behavior of the FP in Sec. II. Then, in Sec. III, three samples of order parameter are produced by the 3D three-state Potts model, where the CP, the point of the first-order PT line, and the point of the crossover region are all well defined. In Sec. IV, we demonstrate that in the plane of T and a, the contour plot of defined width precisely locates the position of the FP in three given samples, respectively. In Sec. V, a possible application of the method at the Relativistic Heavy Ion Collider (RHIC) Beam Energy Scan (BES) is discussed. Finally, a summary is given in Sec. VI.

II. DESCRIPTION OF FIXED POINT

In Figs. 1(b) and 1(d), at a given T, when T approaches $T_{\rm C}$ (or $T_{\rm tr}$) in value, the points of curves for different sizes approach each other, allowing the formation of an intersection point. When T deviates from $T_{\rm C}$ (or $T_{\rm tr}$), all points separate from each other. In order to quantify the relative distance between the points, we define, at a given a, the width of all size scaled observables $(Q(T, L)L^a)$ to be the square root of their variance, i.e.,

$$D(T, a) = \sqrt{\frac{\Delta S_{Q(T,L)L^a}}{N_L - 1}}. \tag{2}$$

Here, $D(T, a)$ varies with T and a, and N_L is the number of sizes. $\Delta S_{Q(T,L)L^a}$ is the error weighted variance of all scaled observables to their mean position, i.e.,

$$\Delta S_{Q(T,L)L^a} = \sum_{i=1}^{N_L} \frac{\left[Q(T, L_i)L_i^a - \langle Q(T, L)L^a\rangle\right]^2}{\omega_i^2}. \tag{3}$$

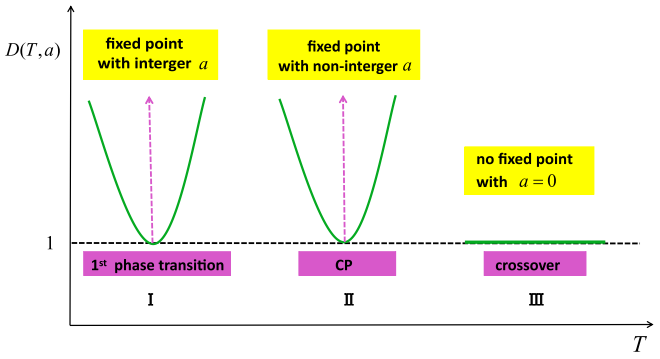

FIG. 2. $D(T, a)$ nearby the temperatures of the (I) first-order PT, (II) second-order PT, and (III) the crossover region.

$\omega_i = \delta[Q(T, L_i)L_i^a]$ is the error of $Q(T, L_i)L_i^a$. $\langle Q(T, L)L^a\rangle$ is the weighted mean, i.e.,

$$\langle Q(T, L)L^a\rangle = \frac{\sum_{i=1}^{N_L} Q(T, L_i)L_i^a/\omega_i^2}{\sum_{i=1}^{N_L} 1/\omega_i^2}. \tag{4}$$

$D(T, a)$ describes the relative distance of all points to their mean position. When T and a deviate from critical (transitional) values, the points of curves for different sizes move away from each other, and the value of $D(T, a)$ increases. When T and a are both the critical (transitional) values, all points overlap within error. $D(T, a)$ reaches its minimum around unity.

Such defined width is analogous to the χ^2 of curve fitting, where the variance is the measured points of a given curve. The minimum of χ^2 corresponds to the best curve fitting.

In a real experiment, due to the error of observable and other uncertainties, the FP may not be an ideal point, and the minimum of $D(T, a)$ may be larger than unity. Nevertheless, if there is a FP in the T-a plane, the $D(T, a)$ will change with T and a and converge to a minimum. This converging trend of $D(T, a)$ is essential for forming a FP.

At three different regions of phase plane, $D(T, a)$, T and a are expected to be cases I, II, and III, respectively, as shown in Fig. 2.

In case I, T is low. $D(T, a)$ has a minimum at the transitional T, where the SER a is an integer. It characterizes the FP of the first-order PT.

In case II, T is in the middle. $D(T, a)$ has also a minimum at the T_C, and the SER a is a fraction, in contrast to case I. It characterizes the FP of the second-order PT, i.e., the CP.

In case III, T is high. $D(T, a)$ is a constant, independent of T, and the SER a is zero. The observable is independent of system size. It characterizes the FP of the crossover region.

In the following, we show in practice how to locate the FP and determine its T_{FP} and a_{FP}.

III. THREE SAMPLES OF THE POTTS MODEL

The same as QCD with finite temperature and infinite quark mass, the 3D three-state Potts model has Z(3) global symmetry [26–29]. The external magnetic field in the Potts model plays the role of the quark mass in the finite-temperature QCD. At vanishing external field, the temperature-driven PT has been proven to be of the first order [30,31]. As the external field increases, the first-order PT weakens and ends at the CP, $(1/T_C, h_C) = (0.54938(2), 0.000775(10))$ [18,27], which belongs to a 3D Ising universality class, the same as deconfining and chiral CPs in QCD. Above the critical temperature, the transition is a crossover [25].

The 3D three-state Potts model is described in terms of spin variable $s_i \in 1, 2, 3$, which is located at sites i of a cubic lattice with size $V = L^3$. The Hamiltonian of the model is defined by [18,32]

$$H = \beta E - hM. \tag{5}$$

The partition function is

$$Z(\beta, h) = \sum_{\{s_i\}} e^{-(\beta E - hM)}, \tag{6}$$

where $\beta = 1/T$ is the reciprocal of temperature, and $h = \beta H$ is a normalized external magnetic field. E and M denote the energy and magnetization respectively, i.e.,

$$E = -J\sum_{\langle i,j\rangle}\delta(s_i, s_j) \text{ and } M = \sum_i \delta(s_i, s_g). \tag{7}$$

Here J is an interaction energy between nearest-neighbor spins $\langle i, j\rangle$ and set to unity in our calculations. s_g is the direction of ghost spin for the magnetization of nonvanishing external field ($h > 0$). For vanishing external field the model is known to have a first-order PT. With increase of the external field, the first-order PT line ends at a CP.

The order parameter of system is defined as

$$m(T, L) = \frac{3\langle M\rangle}{2V} - \frac{1}{2}. \tag{8}$$

However, at the CP, the original operators E and M lose their meaning as T-like and H-like, i.e., symmetry breaking couplings, as those in the Ising model. The order parameter and energylike observable have to be redefined as the combination of the original E and M [18], i.e.,

$$\tilde{M} = M + sE \text{ and } \tilde{E} = E + rM. \tag{9}$$

The Hamiltonian in terms of $\tilde{M}$ and $\tilde{E}$ is

$$H = \tau\tilde{E} - \zeta\tilde{M}, \tag{10}$$

where new couplings are given by

$$\zeta = \frac{1}{1 - rs}(h - r\beta) \text{ and } \tau = \frac{1}{1 - rs}(\beta - sh). \tag{11}$$

Here r and s are mixing parameters and were determined in Ref. [18] by

$$r^{-1} = \left(\frac{d\beta_C(h)}{dh}\right)_{h=h_C} \text{ and } \langle\delta\tilde{M}\cdot\delta\tilde{E}\rangle = 0, \tag{12}$$

with $\delta\tilde{X} = \tilde{X} - \langle\tilde{X}\rangle$ for $X = M$ or E.

The order parameter in terms of τ and ζ is

$$m(\tau, \zeta) = \frac{1}{L^3}[\tilde{M}(\tau, \zeta) - \langle\tilde{M}(\tau_C, \zeta_C)\rangle]. \tag{13}$$

It is the most sensitive observable to the PT. According to Eqs. (12) and (13), it can be written in terms of T and

TABLE I. Parameters of T and a at $D_{\min}(T, a)$ for three samples (corresponding ones from conventional methods are shown in parentheses).

Sample	$D_{\min}(T, a)$	T	a
Second-order PT	1.0291 ± 0.2946	1.82023(1.82023372)	0.583(0.564)
First-order PT	1.5287 ± 0.5591	1.81887(1.8188763)	−0.047(−0.0541)
Crossover	∼1 for all T	1.8256–1.8261	$-0.05 \sim 0.05$

h as

$$m(T, h) = \frac{1}{L^3}[\tilde{M}(T, h) - \langle \tilde{M}(T_c, h_c)\rangle], \tag{14}$$

where $\tilde{M}(T, h) = M(T, h) + sE(T, h)$, and $M(T, h)$ is obtained by Eq. (7) from generated spins at the lattice. The mixing parameter s is estimated from Table 2 of Ref. [18] and Eq. (12).

In the following, we take the observable as the average absolute order parameter over all configurations, i.e.,

$$m(T, h) = \left\langle \left| \frac{1}{L^3}\left[\tilde{M}(T, h) - \langle \tilde{M}(T_c, h_c)\rangle\right] \right| \right\rangle. \tag{15}$$

For fixed external field h, it is the function of temperature and system size, i.e., $m(T, L)$.

Three samples of order parameter are generated at three external fields, i.e., the first-order PT line ($h = 0.0005$ [32]), the CP ($h = 0.000775$ [18,33]), and the crossover region ($h = 0.002$ [32]), respectively. At each of external field, 18 T values are chosen starting from $T_0 = 1.8180$ with $\Delta T = 0.0001$. For a pair of couplings $(\beta = 1/T, h)$, 1×10^5 independent configurations are generated.

The simulation is performed by the Wolff cluster algorithm [34], and the helical boundary conditions are used, where a Ferrenberg-Swendsen reweighting analysis [35] is used to calculate observables at intermediate parameter values. For each case, the simulation is carried out for four different lattice sizes $L = 30$, 40, 50, and 60.

The transitions T and a for the above three samples are listed in parentheses in Table I [18,32]. They are obtained by conventional methods as mentioned in the Introduction [10,16,17].

IV. LOCATING FIXED POINTS

Now, we have three samples, where observables (mean of order parameters) for different T and L are presented. For each sample, we calculate its corresponding width $D(T, a)$ and plot it in the T-a plane.

According to the definition in Eq. (2), the width of the order parameter is

$$D(T, a) = \sqrt{\frac{\Delta S_{m(T,L)L^a}}{N_L - 1}}, \tag{16}$$

where

$$\Delta S_{m(T,L)L^a} = \sum_{i=1}^{N_L} \frac{1}{\omega_i^2}\left[m(T, L_i)L_i^a - \langle m(T, L)L^a\rangle\right]^2. \tag{17}$$

ω_i is the error of $m(T, L_i)L_i^a$. For a given lattice size L, ω_i mainly comes from $m(T, L_i)$ and is estimated by the square root of the variance of $m(T, L_i)$.

$$\langle m(T, L)L^a\rangle = \frac{\sum_{i=1}^{N_L} m(T, L_i)L_i^a/\omega_i^2}{\sum_{i=1}^{N_L} 1/\omega_i^2} \tag{18}$$

is error weighted average. The summation number N_L is equal to 4 for four system sizes $L = 30$, 40, 50, and 60.

The contour plots of $D(T, a)$ in the plane of T and a for three samples are presented in Figs. 3(a)–3(c), where the color bars on the right-hand sides of subfigures indicate the values of $D(T, a)$. The range of a is from −1.2 to 1.15 with interval 0.05. The red and blue zones are minimum and maximum, respectively. The dash-dotted lines indicate the coordinates of T and a corresponding to the minimum of $D(T, a)$.

For the sample with external field $h = 0.000775$, the contour lines in Fig. 3(a) show that $D(T, a)$ gradually converges

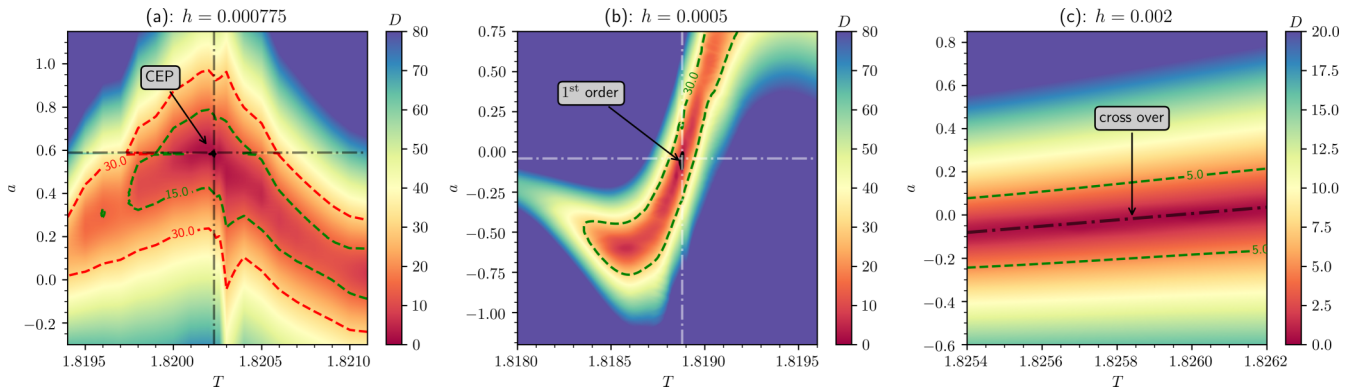

FIG. 3. $D(T, a)$ for three samples with external fields (a) $h = 0.000775$, (b) 0.0005, and (c) 0.002. Dash-dotted lines label the coordinates of $D_{\min}(T, a)$ and dashed lines are isolines.

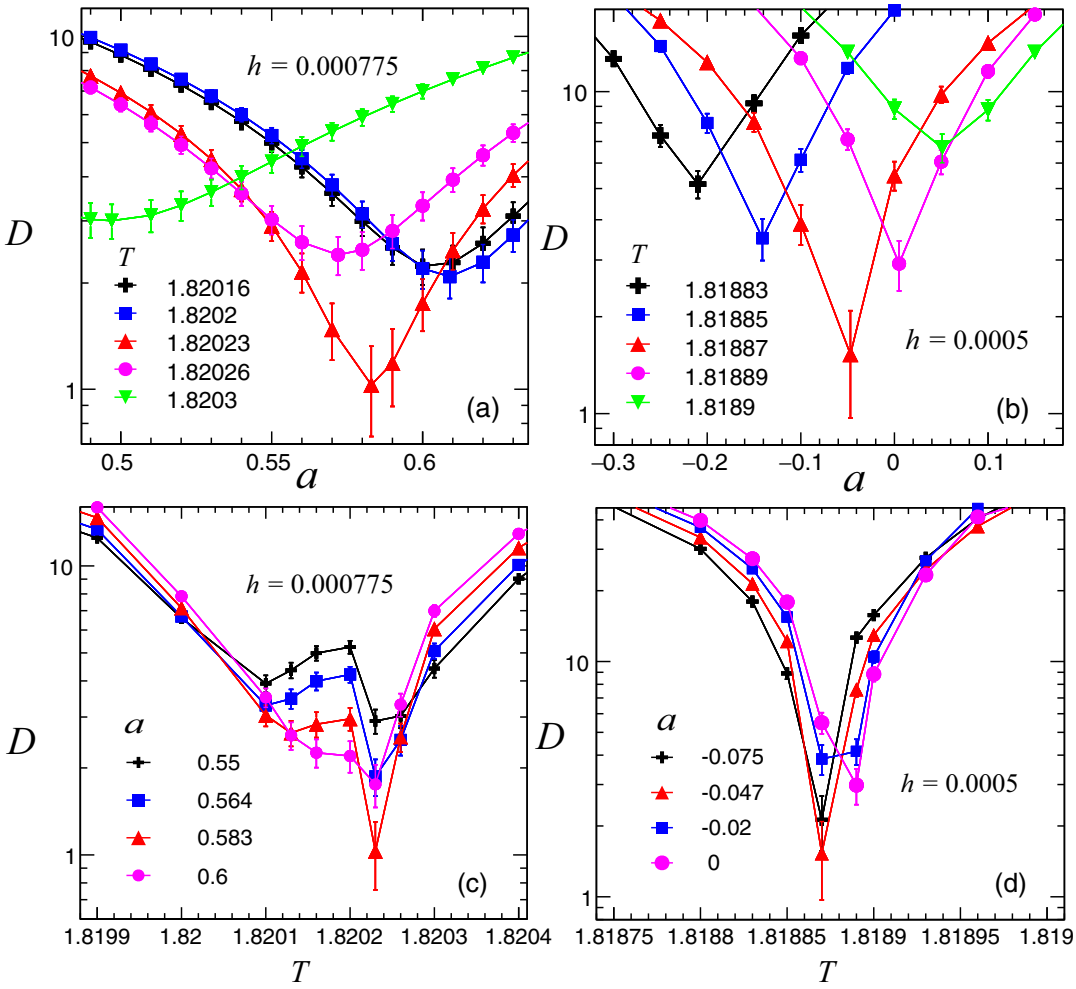

FIG. 4. Projections of $D(T, a)$ on (a, b) exponent ratio and (c, d) temperature axes near (a, c) the critical point and (b, d) the point of the first-order phase transition line.

to a minimum, the red area. This means that the width converges to a minimum at a specified T and a. These are typical features of a FP.

To amplify the fine structure and minimum near the red area, we project $D(T, a)$ to a and T axes, respectively, as shown in Figs. 4(a) and 4(c). In Fig. 4(a), for a given T, there is an a which makes $D(T, a)$ minimum. Among these lines, the minimum of the red line is the smallest one, where $D_{\min} = 1.0291 \pm 0.2946$, and corresponding $T = 1.82023$ and $a = 0.583$. They are very close to 1.82023372 and 0.564, as listed in the parentheses in the second row of Table I.

From the projection along the direction of temperature as shown in Fig. 4(c), for a given ratio a, there is also a minimum $D(T, a)$. The minimum of the red line is the smallest one among them. Its corresponding T and a are the same as those from Fig. 4(a).

These features of $D(T, a)$ and value of a are consistent with the FP of the second-order PT, i.e., the CP, as shown in case II in Fig. 2.

Turning to the sample with external field $h = 0.0005$, the contour lines in Fig. 3(b) also show that $D(T, a)$ gradually converges to a minimum, the red area. This means that all curves of the scaled observable for different sizes are more and more close to each other with the change of T and a, as expected for a FP.

The projection plots of $D(T, a)$ versus a for different T are shown in Fig. 4(b). The curve which has the smallest minimum is the red one with $D_{\min}(T, a) = 1.5287 \pm 0.5591$, $T = 1.81887$, and $a = -0.047$. They are very close to the $T = 1.8188763$, and $a = -0.0541$, as listed in the parentheses in the third row of Table I. Here the order parameter can be considered the first order of susceptibility, i.e., $n = 1$. So $a = (n - 1)d = 0$.

The projection along the direction of T is shown in Fig. 4(d); for a given ratio a, there is also a minimum $D(T, a)$. The smallest minimum gives the same T and a as those from Fig. 4(b). Those are the features of the FP of the first-order PT line, as shown in case I in Fig. 2.

For the sample with external field $h = 0.002$, the contour lines of $D(T, a)$ in Fig. 3(c) are bands parallel to the T axis, in contrast to Figs. 3(a) and 3(b). This implies that $D(T, a)$ is independent of T. Its value is determined by a only. The minimum, the red band, is close to zero. These are the features of the FP of the crossover region, as shown in case III in Fig. 2.

These three examples show that the defined width is very sensitive to T and a. The minimum of $D(T, a)$ precisely

determines the T and a of the FP. Therefore, as long as the FP exists in the T-a plane, the minimum of the defined width can clearly locate it.

The contour area of defined width $D(T, a)$ as shown in Fig. 3 in fact indicates critical or transitional ranges of temperature T and critical exponent ratio a, where all curves for different sizes start to converge toward each other. Out of the area, $D(T, a)$ is big and uniformly blue, i.e., all curves are apart from each other. This contour area for the second-order PT as shown in Fig. 3(a) is obviously larger than that of the first-order PT as shown in Fig. 3(b), where the temperature range is much narrower. Therefore, the PT of the first order is very sensitive to the change of T.

In the critical or transitional range, for a given temperature T (a), there is an a (T) that makes the $D(T, a)$ a minimum, as shown in Fig. 4. This minimum implies that all curves for different sizes are closest to each other at given T (a). Usually this minimum is larger than unity; i.e., all curves are still not overlapped within error. Only for the critical or transitional T (a), the minimum of $D(T, a)$ is the smallest and around unity; i.e., all curves converge to a FP within errors. So defined width well quantifies the behavior of the FP, the ranges of critical or transitional T and a, and the deviation of T and a from the ranges.

On the other hand, if some system sizes are too small for the FSS, their corresponding curves in the plots like Figs. 1(b) and 1(d) will not converge exactly to the FP within error. In that case, the smallest minimum of $D(T, a)$ will be larger than unity. Therefore, $D(T, a)$ is around unity if and only if various system sizes are all properly large and all parameters in the FSS in Eq. (1) are critical or transitional values.

Certainly, a real sample may not be so well represented by the above three samples. It depends on the observable, the covered area of the phase plane, and experimental settings.

First, as we know, some observables, such as energy density and specific heat, may not exactly follow the FSS in the vicinity of T_C [36]. For this kind of observable, additional terms of scaling violation are not negligible [37,38]. The scaling function usually varies with the system size and temperature. There is no FP [37,38].

Second, the suggested contour plot depends on its covered area of the phase plane. If it is far away from the phase boundary, the observable is independent either of temperature or system size [32], and the plot is largely blue, as shown in Fig. 3. If it approaches the phase boundary, or the transition temperature, the plot may show some contour areas which are similar to a part of Figs. 3(a), 3(b), or 3(c). Therefore, the contour plot of defined width is helpful in exploring FPs of the phase boundary.

It should also be noticed that due to the error of observables and uncertainties of related parameters in real experimental settings, the minimum of $D(T, a)$ may be larger than unity and vary with experiments. What is more important for the formation of a FP is the trend of $D(T, a)$ converging to a minimum.

V. A POSSIBLE APPLICATION

One of the main goals of contemporary BES at RHIC and future Compressed Baryonic Matter (CBM)/Facility of Antiproton and Ion Research (FAIR) and Nuclotron-based Ion Collider fAcility (NICA) experiments is to study the critical end point (CEP) in the QCD phase diagram in terms of existence and location [5–8,39–41]. As incident energy of the collision ($\sqrt{s_{NN}}$) changes, temperature T and baryon chemical potential μ_B of the formed system in the phase plane change accordingly. How they change is directed by the simplification of thermal model descriptions of the freeze-out region [15,42,43]. Therefore, the purpose of the BES program is to scan the observable in the T and μ_B plane.

Due to the small volume and the short lifetime of the quark-gluon plasma (QGP) formed in heavy-ion collisions, the CEP, if appears, will be blurred. Critical fluctuations are severely influenced by finite volume, as well as finite time. Due to finite evolution time and critical slowing down, the system may not reach thermal equilibrium or pass the CEP [44,45]. The nonequilibrium evolution depends on the given dynamics which are currently unclear, and should be examined with caution.

For a restricted volume which is not very small, the singularity of generalized susceptibility χ_i is limited into a finite peak with modified position and width [46,47]. With the decrease of volume size, the peak position shifts towards lower temperature and larger chemical potential [48–50]. It is the so called pseudocritical point. The precise position of the CEP has to be determined by the FSS of the observable [15,51,52].

The FSS of several observables in relativistic heavy-ion collisions has been studied [14,15,53–55]. In this paper, we suggest locating the FP by the newly defined width of all points of scaled observables for different sizes at a given T and a. The minimum of the width in the T-a plane is the location of the FP. Graphing with the width allows us to easily locate the FP (should it exist in the phase plane) without selecting the best scaling plot of the observables, thus eliminating inaccuracies introduced by human observation. The value of a_{FP} indicates that the FP is a CP, a point of the first-order PT line, or a point in the crossover region. So classifying the observed FP becomes possible.

As we know, there are still numbers of uncertainties in applying the FSS in relativistic heavy-ion collisions [14,15]: whether the observable is properly chosen, whether the phase boundary is covered by the BES, and whether the system size can be correctly estimated.

The system size is related to the given centrality of heavy-ion collisions. It may be influenced by the incident energy as well. The relations between them have not been set up quantitatively, and should be studied carefully in the future. Currently, the radii of Hanbury Brown–Twiss (HBT) interferometry only provides a rough estimation [14,56–58].

In particular, it is difficult to define an appropriate observable in heavy-ion collisions. Although the order parameter of chiral and deconfining PT is well defined from the theoretical side [7], its corresponding observable is still not known. Certainly, it is better to measure observables, like the order parameter in the Potts model, or the susceptibility, as discussed at the end of the above section. However, it is impossible to know beforehand if the observable is analogous with the order parameter, the susceptibility, or the specific heat.

Nevertheless, it should be helpful and worthwhile to try the method by suggested observables, such as event-by-event

fluctuations of the net baryon number, the electric charge, or the strangeness of the heavy-ion system [59–61], and explore the possible FP at the RHIC BES as was delineated in Refs. [14,15].

VI. SUMMARY AND CONCLUSIONS

In the finite-size scaling, the critical point is a fixed point, where all scaled observables of different system sizes intersect. A fixed point also exists on the first-order PT line and can be generalized to the crossover region. Their corresponding scaling exponent ratios are fraction, integer, and zero, respectively.

To quantify the features of the FP, we define, at a given T and a, the width of scaled observables for different sizes. When $T = T_{\mathrm{FP}}$ and $a = a_{\mathrm{FP}}$, the defined width reaches its minimum.

Then, using the 3D three-state Potts model, we produce three samples at three external fields. These three samples contain, respectively, the CP, the point of the first-order PT line, and the point of the crossover region. The temperature covers the whole possible range. We calculate the widths of order parameters in all three samples, and plot them in the T-a plane.

The contour plot of defined width clearly shows the critical or transitional ranges of temperature and critical exponent ratio. The minimum of defined width locates precisely the position of the FP in three samples, respectively. These demonstrate the method is effective and precise in locating all three categories of FP. The defined width well quantifies the behavior of the FP.

Therefore, from simply scanning the observable in the phase plane, the FP can be well located by defined width. Finally, a possible application at the RHIC BES is discussed. It should be helpful in locating the FP of QCD PT from the experimental side.

ACKNOWLEDGMENTS

We are grateful to Dr. Xiaosong Chen for drawing our attention to the field. This work is supported in part by the Major State Basic Research Development Program of China under Grant No. 2014CB845402, and the Ministry of Science and Technology (MoST) under Grant No. 2016YFE0104800.

[1] J. B. Elliott, L. G. Moretto, L. Phair, G. J. Wozniak, L. Beaulieu, H. Breuer, R. G. Korteling, K. Kwiatkowski, T. Lefort, L. Pienkowski, A. Ruangma, V. E. Viola, and S. J. Yennello (ISiS Collaboration), Phys. Rev. Lett. **88**, 042701 (2002).
[2] M. Kleine Berkenbusch, W. Bauer, K. Dillman, S. Pratt, L. Beaulieu, K. Kwiatkowski, T. Lefort, W.-c. Hsi, V. E. Viola, S. J. Yennello, R. G. Korteling, and H. Breuer, Phys. Rev. Lett. **88**, 022701 (2001).
[3] D. Achlioptas, R. M. D'Souza, and J. Spencer, Science **323**, 1453 (2009).
[4] A. A. Saberi, Phys. Rep. **578**, 1 (2015).
[5] M. M. Aggarwal *et al.* (STAR Collaboration), arXiv:1007.2613.
[6] STAR Collaboration, BES-II white paper (2014), https://drupal.star.bnl.gov/STAR/starnotes/public/sn0598.
[7] C. S. Fischer, Prog. Part. Nucl. Phys. **105**, 1 (2019).
[8] S. Gupta, X. Luo, B. Mohanty, H. G. Ritter, and N. Xu, Science **332**, 1525 (2011).
[9] M. Fukugita, H. Mino, M. Okawa, and A. Ukawa, J. Stat. Phys. **59**, 1397 (1990).
[10] K. Binder, *Finite Size Effects at Phase Transitions*, edited by H. Gausterer and C. B. Lang (Springer, Berlin, 1992), pp. 59–125.
[11] M. E. J. Newman and G. T. Barkema, *Monte Carlo Methods in Statistical Physics* (Oxford University Press, Oxford, 1999).
[12] V. Privman, *Finite Size Scaling and Numerical Simulation of Statistical Systems* (World Scientific, Singapore, 1990).
[13] J. Cardy, *Scaling and Renormalization in Statistical Physics* (Cambridge University Press, Cambridge, UK, 1996).
[14] R. A. Lacey, Phys. Rev. Lett. **114**, 142301 (2015).
[15] E. S. Fraga, L. F. Palhares, and P. Sorensen, Phys. Rev. C **84**, 011903(R) (2011).
[16] K. Binder, Phys. Rev. Lett. **47**, 693 (1981).
[17] K. Binder, Z. Phys. B **43**, 119 (1981).
[18] F. Karsch and S. Stickan, Phys. Lett. B **488**, 319 (2000).
[19] O. Riordan and L. Warnke, Science **333**, 322 (2011).
[20] M. E. Fisher, Rev. Mod. Phys. **46**, 597 (1974).
[21] K. Wilson, Phys. Rep. **12**, 75 (1974).
[22] M. E. Fisher and A. N. Berker, Phys. Rev. B **26**, 2507 (1982).
[23] J. M. J. van Leeuwen, Phys. Rev. Lett. **34**, 1056 (1975).
[24] B. Nienhuis and M. Nauenberg, Phys. Rev. Lett. **35**, 477 (1975).
[25] Y. Aoki, G. Endrodi, Z. Fodor, S. D. Katz, and K. K. Szabo, Nature (London) **443**, 675 (2006).
[26] T. A. DeGrand and C. E. DeTar, Nucl. Phys. B **225**, 590 (1983).
[27] A. M. Polyakov, Phys. Lett. B **72**, 477 (1978).
[28] L. Susskind, Phys. Rev. D **20**, 2610 (1979).
[29] A. Patel, Nucl. Phys. B **243**, 411 (1984).
[30] H. W. J. Blöte and R. H. Swendsen, Phys. Rev. Lett. **43**, 799 (1979).
[31] W. Janke and R. Villanova, Nucl. Phys. B **489**, 679 (1997).
[32] X. Pan, M. Xu, and Y. Wu, J. Phys. G **42**, 015104 (2015).
[33] S. Kim, P. de Forcrand, S. Kratochvila, and T. Takaishi, Proc. Sci. **LAT2005**, 166 (2005).
[34] U. Wolff, Phys. Rev. Lett. **62**, 361 (1989).
[35] A. M. Ferrenberg and R. H. Swendsen, Phys. Rev. Lett. **61**, 2635 (1988).
[36] C. Domb, M. S. Green, and J. L. Lebowitz, *Phase Transitions and Critical Phenomena, Volume 14*, edited by C. Domb, M. S. Green, and J. L. Lebowitz (Academic Press, New York, 1991).
[37] J. Engels and F. Karsch, Phys. Rev. D **85**, 094506 (2012).
[38] H. W. J. Blöte, E. Luijten, and J. R. Heringa, J. Phys. A: Math. Gen. **28**, 6289 (1995).
[39] F. Becattini, M. Bleicher, T. Kollegger, M. Mitrovski, T. Schuster, and R. Stock, Phys. Rev. C **85**, 044921 (2012).
[40] V. D. Kekelidze, J. Instrum. **12**, C06012 (2017).
[41] H. Stoecker and C. Sturm, Nucl. Phys. A **862**, 92 (2011).
[42] J. Cleymans, H. Oeschler, K. Redlich, and S. Wheaton, Phys. Rev. C **73**, 034905 (2006).
[43] A. N. Tawfik, Int. J. Mod. Phys. A **29**, 1430021 (2014).

[44] A. Bzdak, V. Koch, and N. Strodthoff, Phys. Rev. C **95**, 054906 (2017).
[45] B. Berdnikov and K. Rajagopal, Phys. Rev. D **61**, 105017 (2000).
[46] C. Weber, L. Capriotti, G. Misguich, F. Becca, M. Elhajal, and F. Mila, Phys. Rev. Lett. **91**, 177202 (2003).
[47] P. Olsson, Phys. Rev. B **55**, 3585 (1997).
[48] L. F. Palhares, E. S. Fraga, and T. Kodama, J. Phys. G **38**, 085101 (2011).
[49] R.-A. Tripolt, J. Braun, B. Klein, and B.-J. Schaefer, Phys. Rev. D **90**, 054012 (2014).
[50] J. Braun, B. Klein, and B.-J. Schaefer, Phys. Lett. B **713**, 216 (2012).
[51] Y. Wu, L. Chen, and X. S. Chen, Proc. Sci. **CPOD2009**, 036 (2009).
[52] C. Lizhu, X. S. Chen, and W. Yuanfang, arXiv:0904.1040.
[53] R. A. Lacey, Nucl. Phys. A **956**, 348 (2016).
[54] R. A. Lacey, P. Liu, N. Magdy, B. Schweid, and N. N. Ajitanand, arXiv:1606.08071.
[55] N. G. Antoniou, F. K. Diakonos, X. N. Maintas, and C. E. Tsagkarakis, Phys. Rev. D **97**, 034015 (2018).
[56] D. H. Rischke and M. Gyulassy, Nucl. Phys. A **608**, 479 (1996).
[57] T. Csorgo and B. Lorstad, Phys. Rev. C **54**, 1390 (1996).
[58] S. Chapman, P. Scotto, and U. W. Heinz, Phys. Rev. Lett. **74**, 4400 (1995).
[59] M. A. Stephanov, Phys. Rev. Lett. **102**, 032301 (2009).
[60] M. Cheng *et al.*, Phys. Rev. D **79**, 074505 (2009).
[61] C. Athanasiou, K. Rajagopal, and M. Stephanov, Phys. Rev. D **82**, 074008 (2010).